Accepted Article Preview: Published ahead of online publication

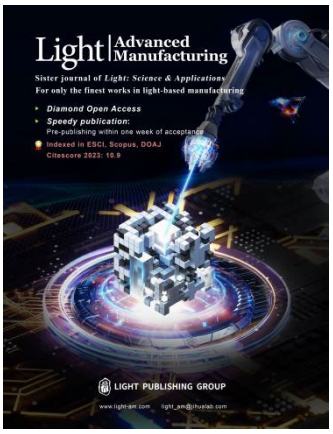

Microring resonator as a Rayleigh mirror for broadband laser-cavity comb generation

Aram A. Mkrtchyan, Anastasia S. Netrusova, Mikhail S. Mishevsky, Zohran Ali, Nikita Yu. Dmitriev, Kirill N. Minkov, Dmitry A. Chermoshentsev, Albert G. Nasibulin, Igor A. Bilenko and Yuriy G. Gladush

Cite this article as: Aram A. Mkrtchyan, Anastasia S. Netrusova, Mikhail S. Mishevsky, Zohran Ali, Nikita Yu. Dmitriev, Kirill N. Minkov, Dmitry A. Chermoshentsev, Albert G. Nasibulin, Igor A. Bilenko and Yuriy G. Gladush. Microring resonator as a Rayleigh mirror for broadband laser-cavity comb generation. *Light: Advanced Manufacturing* accepted article preview 23 June, 2026; doi: 10.37188/lam.2026.108

Received 4 March 2026; revised 17 June 2026; accepted 22 June 2026;
Accepted article preview online 23 June 2026

Microring resonator as a Rayleigh mirror for broadband laser-cavity comb generation

Aram A. Mkrtchyan[1], Anastasia S. Netrusova[1], Mikhail S. Mishevsky[1], Zohran Ali[1], Nikita Yu. Dmitriev[2], Kirill N. Minkov[2], Dmitry A. Chermoshentsev[2,3], Albert G. Nasibulin[1], Igor A. Bilenko[2] and Yuriy G. Gladush[1*]

[1] Skolkovo Institute of Science and Technology, 30 Bolshoy Boulevard, building 1, Moscow, 121205, Russia.

[2] Russian Quantum Center, 30 Bolshoy Boulevard, building 1, Moscow, 121205, Russia

[3] Moscow Institute of Physics and Technology, (National Research University), Dolgoprudny 141700, Russia

These authors contributed equally: Aram A. Mkrtchyan, Anastasia S. Netrusova

*y.gladush@skol.tech

Abstract

Microresonator frequency combs typically require multiple coupling paths or auxiliary stabilisation elements, which can increase system complexity and complicate scalable photonic integration. Herein, we introduce a self-starting comb architecture in which a single-bus microring resonator, placed within a simple laser cavity comprising only an active fibre and an end mirror, serves as a nonlinear frequency-selective mirror. In our configuration, the optical feedback required to form the laser cavity emanates from resonant Rayleigh backscattering in the microring itself, thus avoiding multiport coupling and external frequency scanning for comb initiation. Using this approach, we experimentally observed self-starting coherent frequency combs with a 1 THz repetition rate, no detectable residual pump, and broadband spectra exceeding 500 nm at a central wavelength of 1550 nm. We verified the concept of integrated Si_3N_4 microring resonators and crystalline MgF_2 toroidal microresonators coupled via tapered fibres, thereby confirming the feedback mechanism. The reflective single-bus topology exhibits robust performance and reduces alignment sensitivity compared with multiport coupling schemes used in some frequency comb implementations. With the further development of active waveguide integration, this architecture may offer a path toward more practical and efficient frequency comb sources in future photonic systems.

Keywords: Self-starting laser, nonlinear feedback, laser-cavity soliton, Rayleigh scattering, frequency comb, Kerr nonlinearity

Introduction

Advancements in optical frequency comb generation[1–4] using high-quality (high-Q) microring resonators (MRRs) have led to numerous breakthroughs in metrology,[5–14] spectroscopy,[15,16] communications,[17–20] quantum computing,[21] quantum data processing,[22] and quantum sources.[23,24] For many applications, coherent frequency combs that form dissipative cavity solitons in the time domain should be generated. Solitons are solitary waves that self-balance nonlinear phase shift, dispersion, losses, and energy flow.[25–30] However, the practical implementation of on-chip soliton generation still encounters considerable challenges. The traditional method of soliton generation involves catching the soliton 'step' by scanning through the cavity resonance with a narrow-line laser. This procedure is nontrivial, prohibits self-starting,[26,31–33] and suffers from a low pump-to-comb conversion efficiency, which typically does not exceed 5% for bright solitons.[29,34–36]

Several approaches have been proposed to overcome these limitations, including modifying the microcavity and coupling the pump laser to the cavity through optical feedback.[37] Helgason *et al.* demonstrated a technique of inducing a controllable frequency shift in a selected cavity resonance using two linearly coupled anomalous-dispersion microresonators, achieving a conversion efficiency of 50%.[38] To address the self-starting challenge, Yu *et al.* proposed an edgeless photonic crystal resonator that enables spontaneous soliton formation instead of Turing patterns.[39] Another common but intricate technique is pumping an MRR with an electro-optically modulated continuous-wave (CW) external laser at a precisely selected frequency, which was successfully demonstrated on a lithium niobate platform in 2021.[40] A popular and effective approach is the self-injection locking technique, which provides self-starting soliton comb generation[11,41–45] with a CW-to-soliton comb conversion efficiency of up to 40%.[41] Briefly, the laser diode locks to the travelling-wave mode of the microcavity through a back-propagating wave emerging from Rayleigh scattering within the

cavity.[46] In these schemes, the backscattered field is primarily used to stabilise the laser emission frequency to a microresonator mode rather than to form the laser cavity itself. In addition to cavity-soliton generation, self-injection locking is commonly used for narrow-linewidth, low-noise, and frequency-stabilised laser generation.[47–50]

Another elegant technique that simultaneously solves the problems of low energy conversion and lack of self-starting is the integration of a microcavity into a fibre-laser resonator. This concept was first demonstrated in 2012 to achieve stable ultrafast mode locking.[51] By merging a fibre laser and microcavity, Bao *et al.* demonstrated 50-nm-wide laser cavity-soliton combs with 75% power in the comb.[52] Recently, Maxwell *et al.* demonstrated that this system can exhibit self-starting soliton generation that is naturally robust to system perturbations and can spontaneously recover after disruption. This robustness is attributed to the interplay between slow erbium fibre gain saturation and cavity thermal shift.[53] In these studies, the authors used a four-port ring resonator inside a fibre-laser ring cavity. The emission from the fibre laser propagated through one bus waveguide to the microcavity and returned from the drop port to the laser cavity through the other bus waveguide. A similar approach was implemented using high-Q Fabry–Perot resonators, which can operate in the transmittance and reflectance regimes.[54–58]

In this study, we further developed the technique of laser-cavity soliton generation by demonstrating that a high-Q microring resonator can operate as a nonlinear reflective mirror of a fibre-laser cavity. Studies have shown that weak Rayleigh scattering in the resonator mode can be enhanced by an analogue of the Purcell factor, producing a back-propagating wave in the cavity and, under certain conditions, converting a major part of the pump power into it.[59,60] Although this back-propagating field has previously been used for the self-injection locking of a laser diode to a microresonator mode, it plays a different role in our system: The resonantly enhanced backscattered field provides the dominant feedback that closes and sustains the laser cavity. Specifically, we

demonstrated that resonant backscattering from an MRR, operating as a frequency-selective mirror, can provide sufficiently large optical feedback to form a fibre-laser cavity, leading to more than 500-nm-wide self-starting comb formation. This approach enabled us to use a single-bus waveguide MRR, which simplifies fabrication and reduces losses compared with four-port cavity coupling, thereby maintaining a higher loaded Q-factor and resulting in comb formation with improved spectral properties. To prove the general applicability of this approach and to exclude parasitic reflections as a feedback source, in addition to the integrated MRR, we demonstrated self-starting comb generation in a crystalline MgF_2 toroidal microcavity coupled via a tapered fibre. The tapered-fibre configuration minimises the interface reflections and confirms that the observed feedback originates from microresonator backscattering rather than facet reflections. This approach can be very efficient for robust laser-cavity comb generation with microcavities requiring prism or tapered-fibre coupling and in photonic circuits where the microring is combined with an integrated amplifier.[61–64]

Results

Backward-propagating wave formation is a complex process defined by the relationship between microring resonator parameters, namely, the intrinsic loss (κ_0), coupling rate (κ_C), and backward-wave coupling rate (γ).[60] The MRR used in this study had a 1 THz free spectral range (FSR), an approximately 1 million Q-factor, anomalous second-order dispersion, and the following relationship between its parameters: $\kappa_0<\kappa_C<\gamma<\kappa_0+\kappa_C$ (see the characterisation section for details). At a low pump power, this relationship guarantees a prominent back-propagating wave without significant mode splitting. When the power is sufficiently high for comb formation, a back-propagating comb also forms with a spectrum similar to that of forward propagation, which was observed under an external tuneable CW laser pump (Supplementary Fig. S1).

We used the MRR to form a fibre laser cavity by edge-coupling the chip with the MRR to a polarisation-maintaining (PM) Er-doped fibre amplifier (EDFA) and

introducing a fully reflecting gold mirror on the other side (Fig. 1a). Additionally, the cavity includes a PM-WDM with a 980 nm laser diode and a pair of fibre connectors to simplify the coupling alignment. The total laser cavity length is 3.2 m, corresponding to an FSR of 32.5 MHz. At a threshold pump power of 43 mW, laser generation starts at the wavelength of one of the resonances owing to the build-up of the back-propagating wave in the MRR. As the pump power increases, the optical comb grows, reaching a width of more than 500 nm at the maximum available pump power of 500 mW, corresponding to 91 mW in the fibre before the chip and an output comb power of 16 mW in the bus waveguide (Fig. 1b). The laser can be turned off and turned on, and it immediately recovers the comb state, demonstrating robust operation under external perturbations (see Supplementary Video). This behaviour is similar to that of laser cavity solitons demonstrated earlier with a four-port cavity nested in a fibre laser, where the soliton was manifested as a stable attractor owing to the interaction between slow gain saturation and MRR heating.[53]

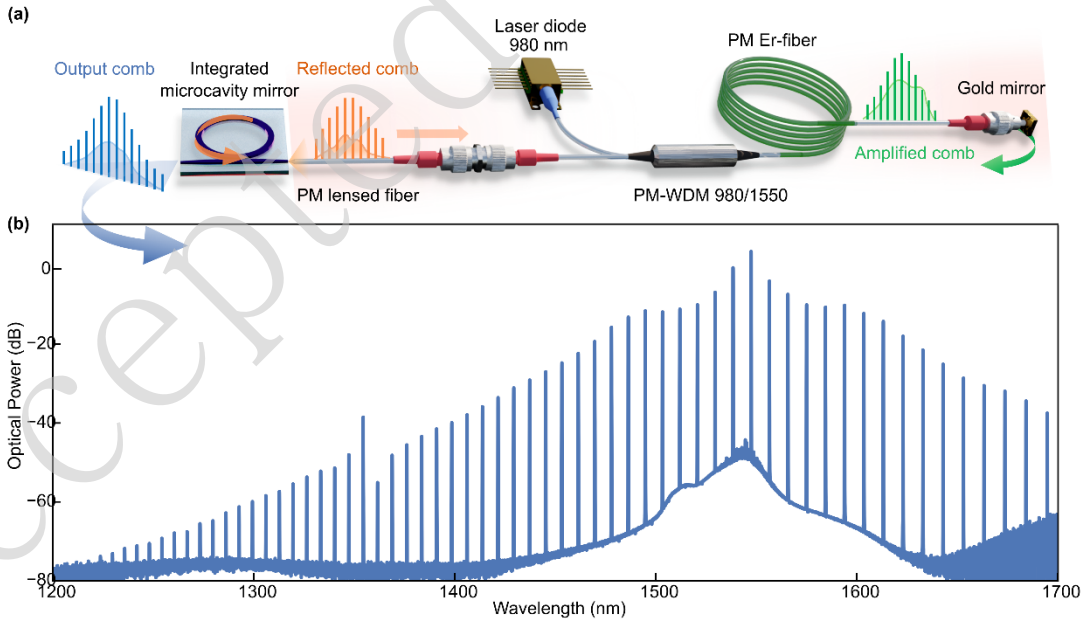

Figure 1. Generation of broadband frequency combs using a high-Q silicon nitride (Si_3N_4) microresonator nested into a fibre-laser cavity in the reflection scheme. a, Schematic illustration of the fibre laser with integrated photonic chip for cavity soliton generation: one-

meter-long polarization-maintaining Er-fibre pumped with a 980 nm laser diode through a broadband wavelength-division multiplexer 980/1550 nm (PM-WDM). All fibres in the system were polarization-maintained and exhibited a second-order dispersion of -23 fs^2 mm^{-1}. Lensed fibres were used to couple light to the chip. The Si_3N_4 microring resonator had a 1 THz repetition rate, nearly 1 million Q- factor, and anomalous dispersion. **b,** Cavity soliton spectrum with a width exceeding 500 nm at an intracavity power.

We note that our scheme does not include an optical filter or delay line, which are often present in such systems, to ensure self-starting and comb coherence.[51–53,65,66] We observed that, in our system, these elements had a very minimal effect on the generation performance; thus, we eliminated them from the cavity. We suggest that a high FSR (approximately 8 nm at 1560 nm) leaves only a few lines within the gain region, where it exceeds the losses, providing efficient filtering. A brief discussion is provided in the Supplementary Information (Section SI2).

To investigate the fibre intracavity dynamics of the comb, we introduced a 2×2 70/30 coupler into the fibre resonator (Supplementary Fig. S7), which enabled us to track the intracavity back-reflected and amplified combs. It introduces additional losses to the system, reducing the intracavity power while preserving the general behaviour. The optical spectra for the transmitted and reflected combs (Fig. 2a,b) have slight differences while maintaining the triangular shape typical of soliton combs. A small dip in the comb spectrum (Fig. 2a) at approximately 1613 nm can be attributed to the avoided mode crossing, as observed from the resonator transmission spectra (Fig. 5c). The apparent reduction in the reflected comb width results from additional wavelength-dependent losses at the coupler and circulator, which increase significantly away from the elemental operation band. Fig. 2c shows the comb after double propagation through the erbium-doped fibre, demonstrating that significant amplification within the erbium gain spectrum region reduces the comb width. An external commercial amplifier was

used to perform autocorrelation measurements (see Supplementary Information, SI4). The autocorrelation traces clearly showed pulse trains with a repetition rate of 1 THz for the output, reflected, and amplified combs (Supplementary Fig. S4). However, a substantial distortion of the comb spectra by the external amplifier prevented us from determining the pulse width. To address the pulse formation and its characteristics, we modelled the intracavity dynamics using coupled mean field equations for MRR forward-propagating, backward-propagating, and fibre-amplified combs. A detailed description of the model and numerical procedure is provided in the Supplementary Information (Section SI3). The dashed envelopes in Figs. 2 (a–c) correspond to the numerical simulation, which exhibited excellent agreement for output and amplified combs. The insets in Fig. 2 (a,b) show the corresponding modelled pulse trains, which had a bell-on-a-pedestal shape for the intracavity pulses. The pedestal was reproduced if the pulse shape was recovered from the Fourier transform under the assumption of full coherence (see Supplementary Information, SI5). The simulated pulse in the fibre laser section, shown in the inset of Fig. 2c, was much broader than the MRR pulses owing to spectral narrowing after the amplifier.

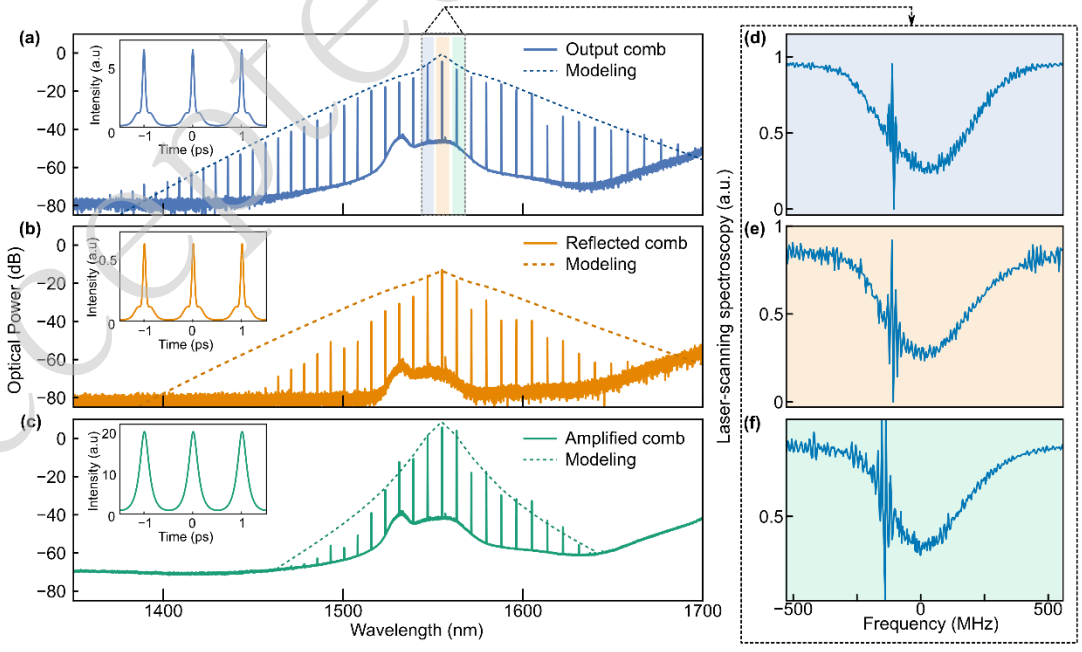

Figure 2. Single soliton comb generation in the hybrid-laser scheme, a–c. Measured output,

a, reflected, **b,** and amplified, **c,** comb spectra. The dashed curves denote the intracavity spectral envelopes computed using the mean-field equations. The insets show pulse trains obtained from the same model, because direct autocorrelation measurements were not feasible owing to an insufficient pulse energy; **d–f,** laser-scanning spectroscopy of the 1542, 1554, and 1562 nm microcavity resonances, respectively, measured for an output comb. All plots indicate the red-detuned state for the central and side modes of the comb.

To further prove the soliton comb operation, we checked whether the comb lines had red detuning using laser-scanning spectroscopy (LSS).[52,65] We introduced an external tuneable 10 kHz linewidth CW laser into the fibre cavity through a fibre optic circulator attached to the additional 70/30 coupler (see Section SI6 in Supplementary Information). The low-power CW laser swept through one of the MRR 'hot' resonances simultaneously with comb generation. For the well-formed comb in Fig. 2a, the beating modes (Fig. 2d–f) clearly indicated a red-shift in the central and two side modes with respect to the cavity resonance, indicating that the system may operate in the soliton regime.[30,67] Note that we always observed only a single mode inside the resonator and observed no hopping between the fibre resonator modes. We concluded that the laser operates in a single supermode, i.e. a sequence of equidistant laser modes with 1 THz separation, which is also evidence for pulsed generation with a repetition rate of 1 THz.

Next, we measured the pump power-dependent spectrum, mode detuning, and fibre intracavity power simultaneously at the chip, as well as the reflected and transmitted positions (Supplementary Fig. S7). The power entering the bus waveguide (green line in Fig. 3a) exhibited a linear dependence on the pump power. This power was converted into a forward-propagating comb (blue area) and backward-propagating comb (red area), whereas the remaining power (green area) corresponded primarily to losses in the MRR. Additionally, we observed that the transmitted and reflected combs exhibited a nonlinear dependence on the pump power.

To investigate the comb formation in more detail, in Fig. 3b, we plotted the

power fractions of the transmitted (blue line) and reflected (red line) combs, as well as the corresponding mode detunings as a function of power inside the bus waveguide. The corresponding comb spectra are shown in Fig. 3c. Below the lasing threshold, almost all the power was transmitted, whereas a small reflection on the order of 1% can be attributed to the reflection from the chip facet (see Supplementary Fig. S8 for the fractions of transmitted and reflected light measured in the fibres). As the power inside the waveguide approached 1 mW, a rapid increase in the reflection to 48% was observed, accompanied by a decrease in the transmitted signal to 10%. LSS measurements showed that in the CW state, the laser mode was blue-detuned with respect to the MRR resonance. However, as the power increased and the comb was excited, the laser supermode shifted to a red-detuned state. This behaviour resembled the comb formation observed in the filter-driven four-wave mixing setup reported by Rowley *et al*.,[53] with a notable difference in that multiple-soliton formation was not observed for this MRR at the available pump power. Interestingly, as the comb developed, the reflected signal dropped considerably to 23%, and the transmitted comb power fraction increased to 36%. We attribute this behaviour to the nonlinear interaction between the forward- and backward-propagating waves through cross-phase modulation.[68,69] Additionally, the fraction of light lost in the MRR can be determined by summing the fractions of the transmitted and reflected light (orange line in Fig. 3b). When the pump power is sufficient to form a CW laser line, the losses approach 40% and remain near this value, independent of the pump power. The gradual change in the losses resembles the shift of the laser supermode through the MRR resonances, with the maximum losses corresponding to the supermode position at the resonance minimum.

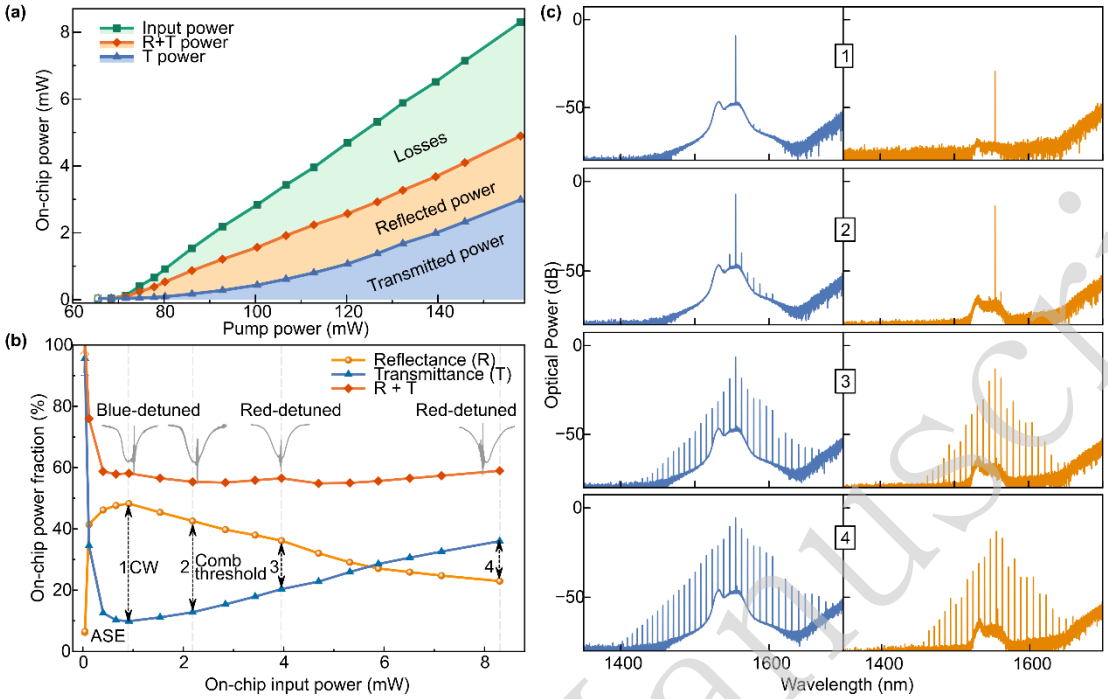

Figure 3. Intracavity dynamic measurements. a, On-chip power (in the bus waveguide) distribution for the transmitted and reflected combs, as well as the power propagated after a double EDFA pass (input), plotted as a function of pump power. **b,** Chip reflection (red) and transmission (blue) as a function of the power in the bus waveguide. The brown line depicts the sum of transmitted and reflected signals, indicating nearly 40% losses in the chip. The numbers correspond to the spectra shown in **c** for different pump powers for transmitted (blue) and reflected (red) combs.

The reflection from the chip facet, reaching 1%, is sufficient to initiate CW laser generation even without the MRR. This raises the question of whether such parasitic reflections affect the start-up dynamics and whether a locking-type feedback mechanism can influence the observed behaviour.[44] Here, our aim is to isolate the feedback origin and verify that self-starting can be triggered by microresonator backscattering alone without relying on parasitic facet reflections. To prove that comb-generation self-starting can be achieved solely with a high-Q MRR mirror, we replaced the chip with a crystalline toroidal microresonator (MgF_2; 10^9 Q-factor, FSR of 35 GHz, and normal dispersion) coupled with a tapered fibre (Fig. 4a). The relatively thick taper with a 3 μm waist was prepared to suppress non-resonant interface reflections (parasitic

feedback) below 10^{-5}. The response of the system to the pump power generally resembled that observed for the integrated MRR. Fig. 4b shows the reflected power from the toroidal resonator as a function of the power incident on the active fibre. When the incident power reached 3 mW (86 mW pump power), the reflection rapidly changed to 0.1%, accompanied by the formation of CW laser emission (see the insets in Fig. 4b for the spectra). A further increase in pump power leads to comb formation.[49,70–72] The system also exhibits self-starting behaviour, which is consistent, even when the pump power is turned off and on. Instead, the observed comb consisted of multiple subcombs associated with different toroidal mode families rather than a single coherent soliton state.[73] The use of a resonator that primarily supports a single mode can reduce the formation of multiple subcombs and favour the emergence of one coherent comb family.[74]

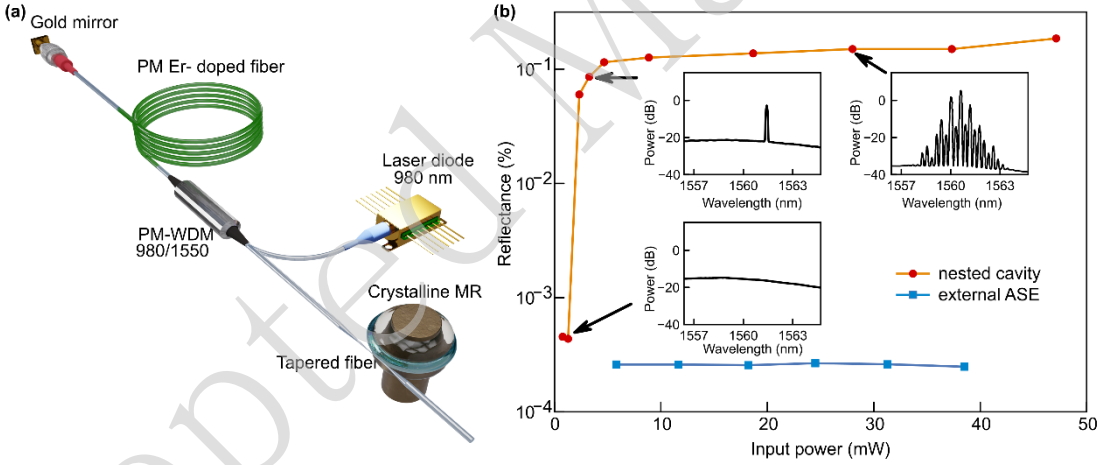

Figure 4. Generation of frequency combs using a high-Q MgF_2 crystalline toroidal microresonator nested into the fibre cavity, where only backward light propagation due to Rayleigh scattering creates feedback. a, Hybrid-laser scheme with the crystalline MgF_2 MRR with 10^9 Q-factor, 35 GHz FSR, and normal dispersion, used to generate whispering gallery modes. **b,** Reflection from crystalline microcavity as a function of power incident from the active fibre (red curve). The corresponding spectra are shown in the insets. The blue curve shows the reflection from an external amplified spontaneous emission (ASE) source, which is independent of the source power.

Discussion

We demonstrated that a ring microcavity can operate as a partially reflecting, nonlinear, frequency-selective mirror that forms a laser cavity for efficient and robust comb generation. In our scheme, the microring resonator plays a dual role: it generates a frequency comb and, through resonantly enhanced Rayleigh backscattering, provides dominant optical feedback that closes and sustains the laser cavity in a reflective configuration, distinct from traditional auxiliary stabilisation paths.

We validated the concept using two resonator platforms: a Si_3N_4 microring resonator with a single-bus waveguide and a crystalline MgF_2 toroidal microresonator coupled with a tapered fibre. In both cases, we observed self-starting operation and recovery of the comb after external perturbations. For the integrated microring, we obtained a 1 THz FSR comb with a spectral width exceeding 500 nm. This coherence was supported by the observed red detuning of the main comb lines, autocorrelation measurements, and agreement with the numerical modelling. This comb exhibited long-term stability and recovered its state when turned off and on. The tapered-fibre MgF_2 experiment, which minimised parasitic interface reflections, further supported the observation that the cavity feedback originates from microresonator backscattering rather than from facet reflections in an integrated coupling interface. Although our current demonstration used a fibre gain medium, the underlying feedback mechanism can be extended to integrated active waveguide platforms, offering potential pathways toward more practical and efficient microcomb sources in future photonic systems.

Materials and Methods

Integrated MRR

The photonic Si_3N_4 chip was fabricated in Ligentec, Switzerland, and contained structures consisting of 25 μm radius microring resonators and bus waveguide (Fig. 5a,b). All structures were fully characterised using a method based on a precalibrated Mach–Zehnder interferometer. [60] The characterisation of the resonator

used in Figs. 2 and 3 included measurements of the microresonator transmission spectrum (Fig. 5d), microresonator dispersion landscape (Fig. 5e), distributions of the Q-factor, intrinsic loss $\kappa_0/2\pi$, coupling rate $\kappa_C/2\pi$, and backward-wave coupling rate (mode splitting) $\gamma/2\pi$ for all resonances in the wavelength range 1510–1620 nm (Fig. 5f). For the central line, the measured parameters were $\kappa_0/2\pi$= 95 MHz, $\kappa_C/2\pi$ = 116 MHz, and $\gamma/2\pi$ = 142 MHz, with a linewidth of 300 MHz. According to the characterisation results, the microring resonator exhibited an anomalous group velocity dispersion of -13.5 fs^2 mm^{-1}, and the pump mode corresponding to the central line of the generated microcomb had $Q \sim 0.9 \times 10^6$ (Fig. 5c).

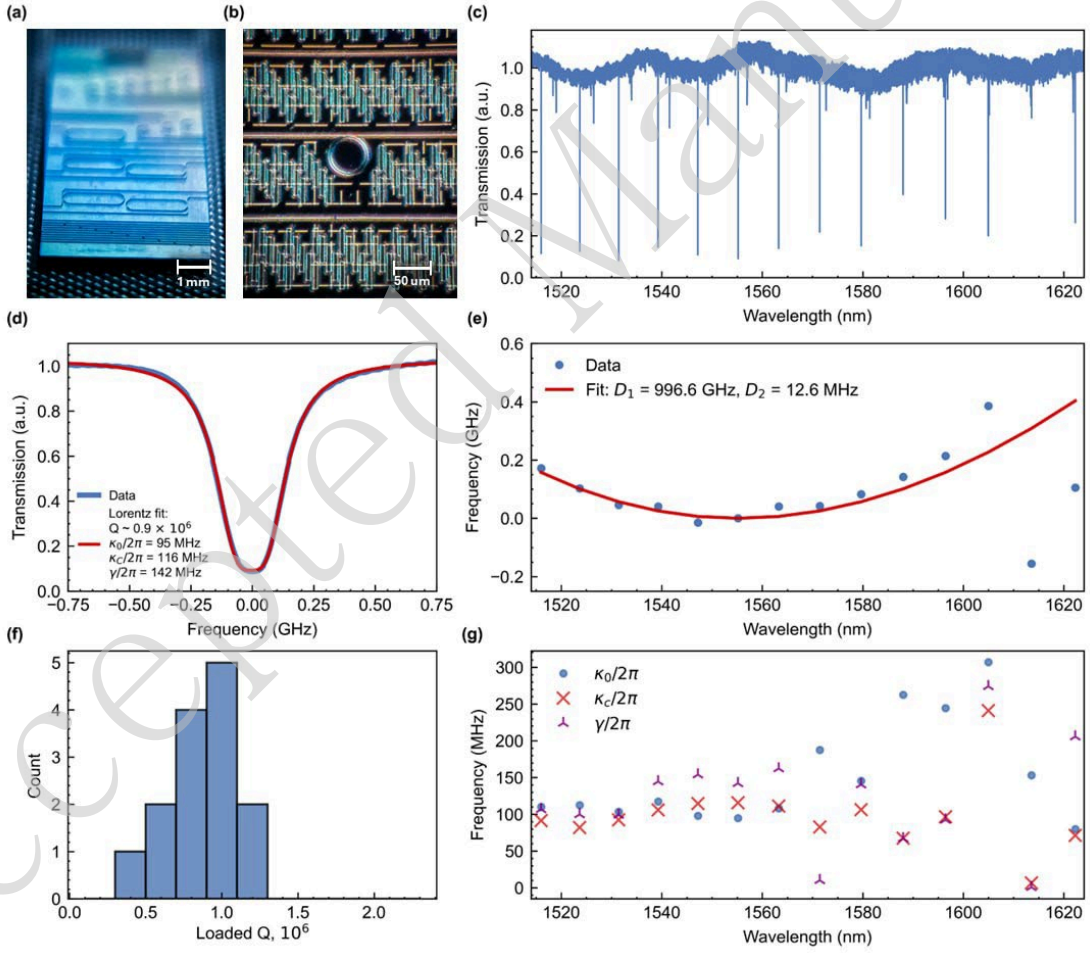

Figure 5. Characterization of the Si_3N_4 microring resonator. a, Photonic chip containing 1 THz microring resonators. **b**, Structure under study consisting of the microring resonator and bus waveguide. **c,** Microresonator mode spectrum. **d,** Parameters of mode corresponding to the

central comb line. **e,** Dispersion landscape (microresonator eigenfrequencies deviation from the uniform FSR grid). **f-g,** Distribution histograms of the Q-factor, intrinsic loss ($\kappa_0/2\pi$), coupling rate ($\kappa_c/2\pi$), and backward-wave coupling rate (mode splitting, $\gamma/2\pi$) for microresonator modes in the range 1510–1620 nm, estimated using a Lorentzian function, with backscattering being considered.

Crystalline microresonator

The microresonator and tapered fibre for coupling were fabricated at the Russian Quantum Center. The resonator was manufactured using magnesium fluoride via diamond turning.[75] The diameter, thickness, and radius of curvature of the resonator were 1.94, 1.0, and 0.35 mm, respectively. The taper was produced from a single-mode fibre (SMF28 Ultra) using a hydrogen flame.[76]

Fibre Laser

The fibre-laser cavity shown in Fig. 2a was assembled from the EDFA spliced to the gold mirror on one side and edge-coupled to the MRR on the other side through the lensed fibre. All fibres used in this study were polarization-maintaining (PM). To create a fully reflecting mirror, gold was sputtered onto the fibre ferrule, resulting in a reflection coefficient of 98%. The EDFA consisted of a 1 m Liekke Er-doped active fibre with an 80 dB/m absorption coefficient at 1530 nm, pumped by a 980 nm laser diode with a maximum power of 500 mW through a 1550/980 wavelength-division multiplexer (1550/980 WDM). The total laser cavity length was 3.2 m, corresponding to a 32.5 MHz FSR.

Measurement Technique

The optical power in the bus waveguide (on-chip power) was calculated by measuring the power of the corresponding fibres (Fig. S7) and multiplying it by the coupling loss, which was 3.5 dB per facet. LSS and chip resonant/out-of-resonance measurements were performed by clean sweeping a narrow-linewidth tuneable Pure Photonics PPCL550 laser through the circulator and the 2.5 μm waist size lensed fibre (AMS

Technologies, PM-lensed fibre TPMJ-3A-1550-8/125-0.25-7-2.5-14-2-AR). The laser power was 17 mW, which resulted in 1.5 mW on the chip. For the LSS, we used a Thorlabs DET08CFC/M 5 GHz photodetector and Tektronix MDO3102 oscilloscope. The average laser power characteristics were measured using Thorlabs S132C power sensors with a wavelength of 1550 nm, corresponding to the central wavelength of the comb. The spectral properties of the optical frequency comb were measured using a DEVISER AE8600 and Yokogawa AQ6370E spectrum analyser with a 600–1700 nm operating window. The temporal characteristics of the solitons were investigated using a Femtochrome FR-103XL autocorrelator at a resolution of 1 fs.

Numerical simulation

We modelled a hybrid fibre-laser–microresonator system using a mean-field formalism developed for laser-cavity-soliton microcombs, in which a Kerr microresonator is coupled to an external fibre loop via discrete supermodes. In our implementation, the microresonator is described by slowly varying envelopes of the clockwise (CW) and counterclockwise (CCW) intracavity fields, and we explicitly include resonant Rayleigh backscattering as a linear coupling term between these counterpropagating modes (Eq. S1–S3). The CCW field is coupled into the fibre cavity, amplified by the gain section, and fed back to the resonator, thereby reproducing the reflective cavity configuration used in the experiments. The coupled mean-field equations are integrated using a Fourier split-step scheme for dispersion and Kerr nonlinearity in the resonator, together with explicit time stepping for linear coupling, loss, and fibre-loop supermodes. The operating points (gain/detuning) were selected using standard modulational-instability (MI) linearisation around the homogeneous steady state, yielding MI maps that guide subsequent time-domain simulations of self-starting single-soliton states. We compared the simulated spectra and time-domain waveforms directly with the experimental data (Fig. 2); the complete parameter set is provided in the Supplementary Table.

Acknowledgements

This study was supported by the Russian Science Foundation (RSF) under Grant No. 25-22-00388.

Author Contributions

Y.G.G., I.A.B., and A.A.M. developed the original research and designed the experiments. A.A.M., A.S.N., Z.A., and N.Y.D. performed the experiments and analysed the data of the integrated chip. A.S.N. and M.S.M. developed the mean-field model and wrote the simulation code. K.N.M. and M.S.M. performed the experiments and analysed the crystalline resonator data. A.A.M. and A.S.N. drafted the manuscript, and Y.G.G., I.A.B., D.A.C., and Y.W. wrote the manuscript. Y.G.G., A.G.N., and I.A.B. supervised this study. All authors participated in the data analysis and contributed to the writing of the manuscript.

Data availability

All data are available from the corresponding authors upon reasonable request.

Conflict of interest

The authors declare no competing interests.

Supplementary information

Supplementary materials are available in the online version and include detailed information on the measurement schemes, numerical modelling, and a video of comb recovery after turning the laser off and on.

References

1. Kippenberg, T. J., Holzwarth, R. & Diddams, S. A. Microresonator-based optical frequency combs. *Science* **332**, 555-559 (2011).

2. Kippenberg, T. J. et al. Dissipative Kerr solitons in optical microresonators. *Science* **361**, eaan8083 (2018).

3. Pasquazi, A. et al. Micro-combs: a novel generation of optical sources. *Physics Reports* **729**, 1-81 (2018).

4. Fortier, T. & Baumann, E. 20 years of developments in optical frequency comb technology and applications. *Communications Physics* **2**, 153 (2019).

5. Savchenkov, A. A. et al. Stabilization of a Kerr frequency comb oscillator. *Optics Letters* **38**, 2636-2639 (2013).

6. Papp, S. B. et al. Microresonator frequency comb optical clock. *Optica* **1**, 10-14 (2014).

7. Del'Haye, P. et al. Phase-coherent microwave-to-optical link with a self-referenced microcomb. *Nature Photonics* **10**, 516-520 (2016).

8. Brasch, V. et al. Self-referenced photonic chip soliton Kerr frequency comb. *Light*: *Science & Applications* **6**, e16202 (2017).

9. Stern, L. et al. Direct Kerr frequency comb atomic spectroscopy and stabilization. *Science Advances* **6**, eaax6230 (2020).

10. Li, B. H. et al. Reaching fiber-laser coherence in integrated photonics. *Optics Letters* **46**, 5201-5204 (2021).

11. Liang, W. et al. High spectral purity Kerr frequency comb radio frequency photonic oscillator. *Nature Communications* **6**, 7957(2015).

12. Lei, F. C. et al. Optical linewidth of soliton microcombs. *Nature Communications* **13**, 3161 (2022).

13. Jin, W. et al. Hertz-linewidth semiconductor lasers using CMOS-ready ultra-high-*Q* microresonators. *Nature Photonics* **15**, 346-353 (2021).

14. Volyanskiy, K. et al. Compact optoelectronic microwave oscillators using ultra-high Q whispering gallery mode disk-resonators and phase modulation. *Optics*

Express **18**, 22358-22363 (2010).

15. Yu, M. J. et al. Silicon-chip-based mid-infrared dual-comb spectroscopy. *Nature Communications* **9**, 1869 (2018).

16. Suh, M. G. et al. Microresonator soliton dual-comb spectroscopy. *Science* **354**, 600-603 (2016).

17. Marin-Palomo, P. et al. Microresonator-based solitons for massively parallel coherent optical communications. *Nature* **546**, 274-279 (2017).

18. Pfeifle, J. et al. Optimally coherent Kerr combs generated with crystalline whispering gallery mode resonators for ultrahigh capacity fiber communications. *Physical Review Letters* **114**, 093902 (2015).

19. Hu, H. et al. Single-source chip-based frequency comb enabling extreme parallel data transmission. *Nature Photonics* **12**, 469-473 (2018).

20. Corcoran, B. et al. Ultra-dense optical data transmission over standard fibre with a single chip source. *Nature Communications* **11**, 2568 (2020).

21. Menicucci, N. C., Flammia, S. T. & Pfister, O. One-way quantum computing in the optical frequency comb. *Physical Review Letters* **101**, 130501 (2008).

22. Lu, H. H. et al. Quantum information processing with frequency-comb qudits. *IEEE Photonics Technology Letters* **31**, 1858-1861 (2019).

23. Kues, M. et al. On-chip generation of high-dimensional entangled quantum states and their coherent control. *Nature* **546**, 622-626 (2017).

24. Reimer, C. et al. Generation of multiphoton entangled quantum states by means of integrated frequency combs. *Science* **351**, 1176-1180 (2016).

25. Herr, T. et al. Temporal solitons in optical microresonators. *Nature Photonics* **8**, 145-152 (2014).

26. Haelterman, M., Trillo, S. & Wabnitz, S. Dissipative modulation instability in a nonlinear dispersive ring cavity. *Optics Communications* **91**, 401-407 (1992).

27. Leo, F. et al. Temporal cavity solitons in one-dimensional Kerr media as bits in an all-optical buffer. *Nature Photonics* **4**, 471-476 (2010).

28. Xue, X. X. et al. Mode-locked dark pulse Kerr combs in normal-dispersion microresonators. *Nature Photonics* **9**, 594-600 (2015).

29. Cole, D. C. et al. Soliton crystals in Kerr resonators. *Nature Photonics* **11**, 671-676 (2017).

30. Xue, X. X. et al. Microresonator Kerr frequency combs with high conversion efficiency. *Laser & Photonics Reviews* **11**, 1600276 (2017).

31. Barland, S. et al. Temporal localized structures in optical resonators. *Advances in Physics*: *X* **2**, 496-517 (2017).

32. Firth, W. Temporal cavity solitons: buffering optical data. *Nature Photonics* **4**, 415-417 (2010).

33. Marconi, M. et al. How lasing localized structures evolve out of passive mode locking. *Physical Review Letters* **112**, 223901 (2014).

34. Wang, P. H. et al. Intracavity characterization of micro-comb generation in the single- soliton regime. *Optics Express* **24**, 10890-10897 (2016).

35. Bao, C. J. et al. Nonlinear conversion efficiency in Kerr frequency comb generation. *Optics Letters* **39**, 6126-6129 (2014).

36. Li, M. et al. Breaking the efficiency limitations of dissipative Kerr solitons using nonlinear couplers. *Science China Physics*, *Mechanics & Astronomy* **67**, 234211 (2024).

37. Yang, Q. F. et al. Efficient microresonator frequency combs. *eLight* **4**, 18

(2024).

38. Helgason, Ó. B. et al. Surpassing the nonlinear conversion efficiency of soliton microcombs. *Nature Photonics* **17**, 992-999 (2023).

39. Yu, S. P. et al. Spontaneous pulse formation in edgeless photonic crystal resonators. *Nature Photonics* **15**, 461-467 (2021).

40. He, Y. et al. Self-starting bi-chromatic $LiNbO_3$ soliton microcomb. *Optica* **6**, 1138-1144 (2019).

41. Dmitriev, N. Y. et al. Hybrid integrated dual-microcomb source. *Physical Review Applied* **18**, 034068 (2022).

42. Stern, B. et al. Battery-operated integrated frequency comb generator. *Nature* **562**, 401-405 (2018).

43. Shen, B. Q. et al. Integrated turnkey soliton microcombs. *Nature* **582**, 365-369 (2020).

44. Voloshin, A. S. et al. Dynamics of soliton self-injection locking in optical microresonators. *Nature Communications* **12**, 235 (2021).

45. Lihachev, G. et al. Platicon microcomb generation using laser self-injection locking. *Nature Communications* **13**, 1771 (2022).

46. Gorodetsky, M. L., Pryamikov, A. D. & Ilchenko, V. S. Rayleigh scattering in high-*Q* microspheres. *Journal of the Optical Society of America B* **17**, 1051-1057 (2000).

47. Dahmani, B., Hollberg, L. & Drullinger, R. Frequency stabilization of semiconductor lasers by resonant optical feedback. *Optics Letters* **12**, 876-878 (1987).

48. Su, Q. S. et al. A self-injection locked laser based on high-*Q* micro-ring

resonator with adjustable feedback. *Journal of Lightwave Technology* **41**, 6756-6763 (2023).

49. Galiev, R. R. et al. Optimization of laser stabilization via self-injection locking to a whispering-gallery-mode microresonator. *Physical Review Applied* **14**, 014036 (2020).

50. Liang, W. et al. Ultralow noise miniature external cavity semiconductor laser. *Nature Communications* **6**, 7371 (2015).

51. Peccianti, M. et al. Demonstration of a stable ultrafast laser based on a nonlinear microcavity. *Nature Communications* **3**, 765 (2012).

52. Bao, H. L. et al. Laser cavity-soliton microcombs. *Nature Photonics* **13**, 384-389 (2019).

53. Rowley, M. et al. Self-emergence of robust solitons in a microcavity. *Nature* **608**, 303-309 (2022).

54. Bunel, T. et al. Brillouin-induced Kerr frequency comb in normal dispersion fiber Fabry Perot resonators. *Nature Communications* **16**, 5160 (2025).

55. Nie, M. M. et al. Turnkey photonic flywheel in a microresonator-filtered laser. *Nature Communications* **15**, 55 (2024).

56. Nie, M. M. et al. Dissipative soliton generation and real-time dynamics in microresonator-filtered fiber lasers. *Light*: *Science & Applications* **11**, 296 (2022).

57. Ibrahimi, Y. et al. Low FSR mode-locked laser based on InP-Si_3N_4 hybrid integration. *Journal of Lightwave Technology* **39**, 7573-7580 (2021).

58. Gao, Z. D. et al. Passive-mode-locked InP/$LiNbO_3$ integrated soliton laser. Proceedings of CLEO: Science and Innovations 2024. Charlotte, North Carolina United States: Optica Publishing Group, 2024, SF3E.6.

59. Mazzei, A. et al. Controlled coupling of counterpropagating Whispering-Gallery modes by a single Rayleigh scatterer: a classical problem in a quantum optical light. *Physical Review Letters* **99**, 173603 (2007).

60. Kippenberg, T. J., Spillane, S. M. & Vahala, K. J. Modal coupling in traveling-wave resonators. *Optics Letters* **27**, 1669-1671 (2002).

61. Liu, Y. et al. A photonic integrated circuit–based erbium-doped amplifier. *Science* **376**, 1309-1313 (2022).

62. Rönn, J. et al. Ultra-high on-chip optical gain in erbium-based hybrid slot waveguides. *Nature Communications* **10**, 432 (2019).

63. Frankis, H. C. et al. Erbium-doped TeO_2 -coated Si_3N_4 waveguide amplifiers with 5 dB net gain. *Photonics Research* **8**, 127 (2020).

64. Van Gasse, K., Wang, R. J. & Roelkens, G. 27 dB gain III–V-on-silicon semiconductor optical amplifier with > 17 dBm output power. *Optics Express* **27**, 293-302 (2019).

65. Bao, H. L. et al. Turing patterns in a fiber laser with a nested microresonator: robust and controllable microcomb generation. *Physical Review Research* **2**, 023395 (2020).

66. Cutrona, A. et al. Nonlocal bonding of a soliton and a blue-detuned state in a microcomb laser. *Communications Physics* **6**, 259 (2023).

67. Yi, X. et al. Soliton frequency comb at microwave rates in a high-*Q* silica microresonator. *Optica* **2**, 1078-1085 (2015).

68. Xu, G. et al. Spontaneous symmetry breaking of dissipative optical solitons in a two-component Kerr resonator. *Nature Communications* **12**, 4023 (2021).

69. Wang, X. Y. et al. Experimental demonstration of self-oscillation microcomb in a mode-splitting microresonator. *Frontiers in Physics* **10**, 908141 (2022).

70. Pavlov, N. G. et al. Soliton dual frequency combs in crystalline microresonators. *Optics Letters* **42**, 514-517 (2017).

71. Shitikov, A. E. et al. Microresonator and laser parameter definition via self-injection locking. *Physical Review Applied* **14**, 064047 (2020).

72. Shitikov, A. E. et al. Optimization of laser stabilization via self-injection locking to a whispering-gallery-mode microresonator: experimental study. *Optics Express* **31**, 313-327 (2023).

73. Grudinin, I. S. & Yu, N. Dispersion engineering of crystalline resonators via microstructuring. *Optica* **2**, 221-224 (2015).

74. Wu, Z. et al. Coexistence of multiple microcombs in monochromatically pumped Si_3N_4 microresonators. *Optics Letters* **47**, 1190-1193 (2022).

75. Min'kov, K. N. et al. Fabrication of high-Q crystalline whispering gallery mode microcavities using single-point diamond turning. *Journal of Optical Technology* **88**, 348-353 (2021).

76. Min'kov, K. N. et al. An automated setup for the manufacture of tapered optical fibers with a submicron diameter. *Instruments and Experimental Techniques* **67**, 390-397 (2024).